

# Automatic Control and Health Monitoring of a 3-Dimensional Overhead Crane with Minimally Required Sensor Devices

Minami Kumarawadu<sup>1</sup><sup>a</sup> and Logeeshan Velmanickam<sup>2</sup><sup>b</sup>

<sup>1</sup>Engineering Design Department, Electro Metal Pressings Pvt Ltd., Panagoda, Sri Lanka

<sup>2</sup>Department of Electrical Engineering, University of Moratuwa, Moratuwa, Sri Lanka

**Keywords:** Overhead Crane, Controller-Observer, Health Monitoring.

**Abstract:** This paper presents a controller-observer scheme for linear position tracking control of the load of an overhead crane in the 3-D space and also investigates the possibility of actuator health monitoring with minimal sensor requirement. This way, admissible position tracking accuracy and system transient behaviour both are achieved only using position sensors. Closed-loop stability of the plant-controller-linear velocity observer system is guaranteed using Lyapunov method. A trajectory planning method is proposed based on standard exponential functions that enables defining the distance to the destination, maximum linear velocities and accelerations in the parameters of the function itself. The methods proposed are validated using computer numerical simulations in the presence of model parameter uncertainties and external disturbances. We also investigate the potential of using observer outputs to improve the early detection of actuator faults.

## 1 INTRODUCTION


Owing to ever increasing operational, maintenance, and safety requirements of industrial multi-motor systems, predictive maintenance (PdM) has received increasing attention. PdM is a data-driven approach to identify operational anomalies and potential equipment defects, enabling timely repairs before failures occur. However, additional sensor and data communication requirements add up to cost and maintenance. To this end, much emphasis has been placed on automatic control and monitoring of systems using minimally required sensor devices (Suzuki and Fujii, 2006, Gowriathan et al., 2023, Gao et al., 2015, Kumarawadu et al., 2007).


3-dimensional overhead cranes are widely used in industry for transportation of heavy loads. Accurate position tracking feedback control of the 3 degrees-of-freedom requires three position sensors. Velocity feedback is required in order to ensure admissible transient performance. As a result, total number of sensor requirement for automatic position tracking control of a 3D overhead crane will be six. Finite difference estimation of the velocity has no theoretical grounds and is also vulnerable to position

measurement noise. Controller-observer schemes can be used to minimize the number of sensors required or to estimate unmeasurable variable for feedback control purposes.

Many controller-observer schemes with guaranteed stability have been proposed for robotic systems (Kumarawadu et al., 2007, Ji et al., 2019) to estimate the robot joint angular velocities. In Kumarawadu and Lee, 2009, a velocity observer has been used to estimate the lateral velocity of self-driving vehicles that is unmeasurable.

In this paper, a controller-observer scheme is used for automatic tracking control with guaranteed closed-loop stability using minimally required sensor devices. This is achieved by a velocity observer that estimates the linear velocities of the moving components in the travel, traverse, and hoist motions. Closed-loop stability of the plant-controller-observer system is guaranteed using Lyapunov method. Our future research includes investigation into how to incorporate the estimated velocity profiles by the observer in identification and localization of anomalies in PdM applications of multiple motor systems. This way, automated health monitoring of engineering systems to be achieved exclusively using

<sup>a</sup> <https://orcid.org/0009-0004-1065-0725>

<sup>b</sup> <https://orcid.org/0000-0003-3767-8280>

the control sensor feedbacks and the estimated motion parameters only.

We also present a trajectory planning method using a combination of exponential functions to ensure smooth tracking trajectories. This is important to ensure minimal swing of the load. In our approach, the desired linear velocity trajectories are planned based on the distance to the destination. Maximum velocity and acceleration are defined using standard exponential functions. As a result, the desired position trajectories can be obtained by simply integrating the smooth varying time function profiles of the desired velocities.

Using frequency domain, correlation, and sensitivity analysis, we investigate the potential of using the position tracking error and the velocity observer output for actuator health monitoring.

This paper is organized as follows: Section 2 presents our feedback controller-linear velocity observer scheme and the trajectory planning approach. Closed-loop stability is established using Lyapunov method. Section 3 presents the simulation results. Actuator fault simulation and analysis is presented in Section 4. Section 5 concludes the paper.

## 2 CONTROLLER-OBSERVER SCHEME

### 2.1 System Equations of Motion

In the 3D overhead crane, travel motion refers to the movement of the entire crane along a fixed runway beam. See Fig. 1. Traverse motion refers to the movement of the crane trolley allowing the crane to position itself horizontally perpendicular to the direction of travel. Hoist motion refers to the vertical movement of the crane's hook-block or lifting mechanism. With reference to an  $x$ - $y$ - $z$  orthogonal set, travel, traverse, and hoist linear motions take place in the  $x \geq 0, y \geq 0$  and  $z \leq 0$  regions, respectively. See Fig. 2.

The model-based controller-observer design approach is based on the linearized equations of motion that ignore the swing dynamics of the load. Let  $M_x, M_y, M_z$  are the travelling, traversing, and hoisting down components of the crane mass. Load mass is  $m$ . By applying Newton's 2<sup>nd</sup> law of motion to the  $x$ -direction,  $y$ -direction, and  $z$ -direction we get  $F_x, F_y, F_z$  are the driving forces,  $D_x, D_y, D_z$  are the viscous friction coefficients, and  $d_x, d_y, d_z$  are the unknown bounded time-varying external disturbance forces for the motions in the  $x, y, z$  directions.

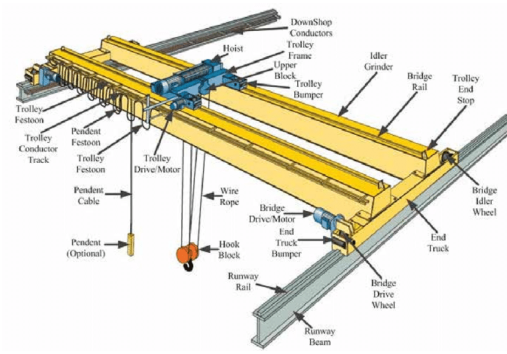


Figure 1: A 3-D overhead crane (Khatamianfar, 2015).

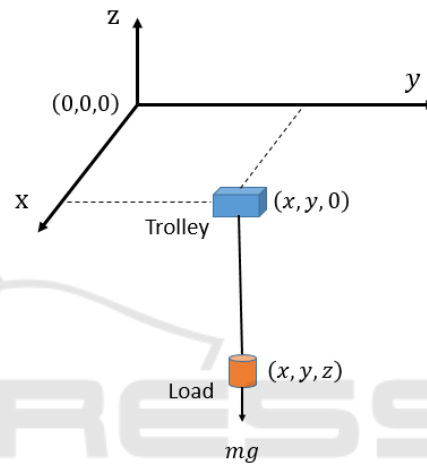


Figure 2: Coordinate system of the 3-D overhead crane.

$$(M_x + m)\ddot{x}(t) + D_x\dot{x}(t) + d_x(t) = F_x(t) \quad (1)$$

$$(M_y + m)\ddot{y}(t) + D_y\dot{y}(t) + d_y(t) = F_y(t) \quad (2)$$

$$(M_z + m)\ddot{z}(t) + D_z\dot{z}(t) - mg + d_z(t) = F_z(t) \quad (3)$$

The disturbance force,  $d(t)$  is a bounded quantity satisfying  $|d(t)| \leq d_M$ , where  $d_M$  is a constant denoting the upper bound. Such disturbance can be considered as energy bounded random noise, which widely exists in practical systems (Jin et al., 2022).

### 2.2 The Controller-Observer Scheme

Automatic controller tracks a planned trajectory to move the load attached to the hook-block of the overhead crane to the final destination in the  $x$ - $y$ - $z$  space and return to the original position. Controller-observer scheme and the stability proof are presented for the  $z$  (hoist) motion. Travel and traverse ( $x$  and  $y$ ) that do not have a  $mg$  term in the dynamics may be considered as special cases.

In the sequel,  $\hat{(\cdot)}$  denotes the estimated value of  $(\cdot)$  and  $\tilde{z} = z - \hat{z}$ . It is assumed that the desired position,  $z_d$ , and its time derivatives,  $\dot{z}_d, \ddot{z}_d$ , are known. The control objective is to regulate the tracking error,  $e = z - z_d$ . Implicit in it are simultaneously keeping the observer estimation error small. Consider the following combined controller-velocity observer system:

Controller:

$$\begin{cases} F = Mv + D\dot{z} - mg \\ v = \ddot{z}_d - k_d(\dot{z} - \dot{z}_d) - k_p(z - z_d) \end{cases} \quad (4)$$

Observer:

$$\begin{cases} \dot{\hat{z}} = r + L_d(z - \hat{z}) \\ \dot{r} = v + L_p(z - \hat{z}) \end{cases} \quad (5)$$

Here,  $M = M_z + m$ . The positive adjustable controller-observer gains,  $k_d, k_p, L_d, L_p$ , are to be chosen by the designer.  $r$  denotes a reference acceleration input, which is obtained by modifying the resolved acceleration with position estimation error. Integrating  $r$  and further modifying it by position estimation error yield the estimated velocity. Consider the controller-observer system defined by (4) and (5) in a closed loop with the controlled system with the plant (3). The closed-loop system can be made to be UUB by suitably selecting the controller-observer gains,  $k_d, k_p, L_d, L_p$ .

Stability proof of the closed-loop system is given in the Appendix.

### 2.3 Trajectory Planning

The desired velocity trajectory for the forward motion is defined as

$$\dot{x}_{d, fwd}(t) = \begin{cases} V(1 - e^{-at}); & 0 \leq t < T \\ Ve^{-a(t-T)}; & T \leq t \leq T + 7 \end{cases} \quad (6)$$

For the return path,  $\dot{x}_{d, return}(t) = -\dot{x}_{d, fwd}(t)$ . Here,  $V$  is the maximum velocity and  $aV$  is the maximum acceleration. Time interval,  $T$ , is selected to match the distance between the starting point and the final destination. For example, the desired velocity trajectories for the roundtrip motion are given in Fig. 3. Here,  $V, aV, T$  are 0.5, 0.5, 20 for travel, 0.4, 0.4, 15 for traverse, and -0.2, -0.2, 5 for hoist motions. When the maximum acceleration and velocity are known, distance travelled can be obtained by time integrating (6) as a function of  $T$ . Hence, the distance travelled can be pre-set by setting the value  $T$ .

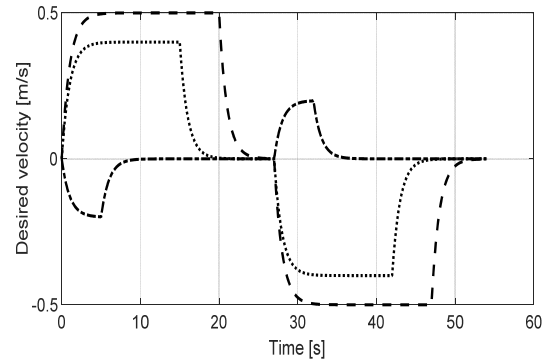


Figure 3: Desired velocity: travel (dashed line), traverse (dotted line), and hoist (dash-dot).

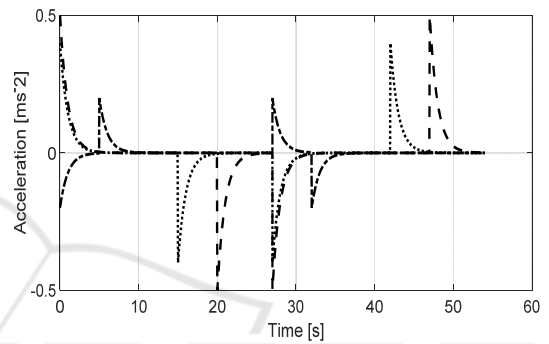


Figure 4: Desired acceleration: travel (dashed line), traverse (dotted line), and hoist (dash-dot).

Desired acceleration trajectories given in Fig. 4 can be obtained by time differentiating the desired velocities. Likewise, desired positions are obtained by time integrating the velocities. As a result, the desired position trajectories and their time derivatives that are required in the control method presented in Section 2.2 can be obtained completely analytically without needing numerical calculus.

## 3 SIMULATION STUDY OF THE HEALTHY SYSTEM

Crane workspace is 12 meters long, 8 meters wide, and 2 meters deep. Its maximum accelerations and velocities are  $2 \text{ m/s}^2$  and  $0.5 \text{ m/s}$  for traveling,  $1.5 \text{ m/s}^2$  and  $0.3 \text{ m/s}$  for traversing, and  $1.5 \text{ m/s}^2$  and  $0.1 \text{ m/s}$  for load hoisting, respectively.

Dynamic model parameters are  $M_x = 1440 \text{ kg}$ ,  $D_x = 400 \text{ kgs}^{-1}$ ,  $M_y = 110 \text{ kg}$ ,  $D_y = 40 \text{ kgs}^{-1}$ ,  $M_z = 20 \text{ kg}$ ,  $D_z = 5 \text{ kgs}^{-1}$ . Load mass,  $m = 150 \text{ kg}$ . Acceleration due to gravity,  $g = 9.81 \text{ ms}^{-2}$ .

The overhead crane system is disturbed by random external disturbance forces formulated by  $d_x(t) = 20 \times (2 \times \text{rand}(1) - 1) \text{ N}$   
 $d_y(t) = d_z(t) = 2 \times (2 \times \text{rand}(1) - 1) \text{ N}$  all the time. Here,  $0 \leq \text{rand}(1) \leq 1$  is a random number.

The hook-block moves from  $(x, y, z) = (0, 0, 0)$  position to  $(10, 6, -1)$  meters with the load and returns to the original position with no load. Controller-observer gains are heuristically set as:  $k_{px} = 10, k_{dx} = 10, L_{dx} = 10, L_{px} = 0.1; k_{py} = 30, k_{dy} = 30, L_{dy} = 10, L_{py} = 0.8; k_{pz} = 35, k_{dz} = 35, L_{dz} = 6, L_{pz} = 0.6$ .

Model parameter uncertainties of 15% is assumed to be in the control law except for the mass of the load, which is known accurately. Following logic is used to reset the model parameter, load mass ( $m$ ), in the control law, (4), for the return motion.

$$m = \begin{cases} m; \dot{x}_d(t) \geq 0 \\ 0; \text{Otherwise} \end{cases} \quad (7)$$

Desired and actual positions are shown in Fig. 5. Fig. 6 presents the position tracking control errors. These figures show small position tracking errors and admissible transient performance. Driving forces are given in Fig. 7.

Actual and observer estimated velocities are compared in Fig. 8. Velocity estimation errors are given in Fig. 9. These figures show very good velocity estimation accuracy and admissible transient performance of the velocity observer.

Fig. 10 shows the position tracking error without load mass parameter resetting as described in (7) in the control law. As it can be seen, hoist position tracking error increases significantly during the return motion without load mass parameter resetting in the control law. Percentage changes in the total mass parameter in the motion dynamics, from the forward motion ( $m = 150 \text{ kg}$ ) to the return motion ( $m = 0$ ) are 9.4%, 27.3%, 57.7%, for the travel, traverse, and hoist motions, respectively. The result in Fig. 9 signifies the importance of load parameter resetting. However, many published work on 3D overhead cranes do not consider the no-load dynamics during the return motion (Lee, 1998).

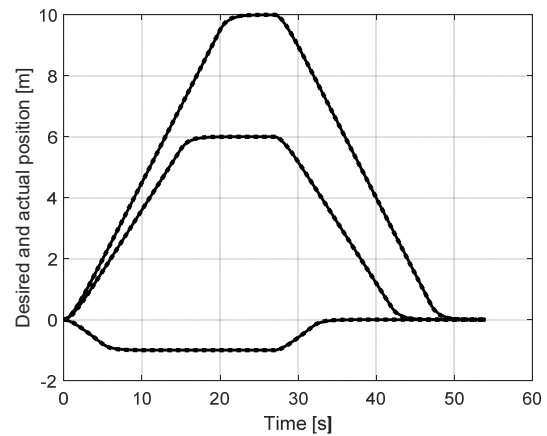


Figure 5: Desired and actual positions: desired (dotted line) and actual (solid line).

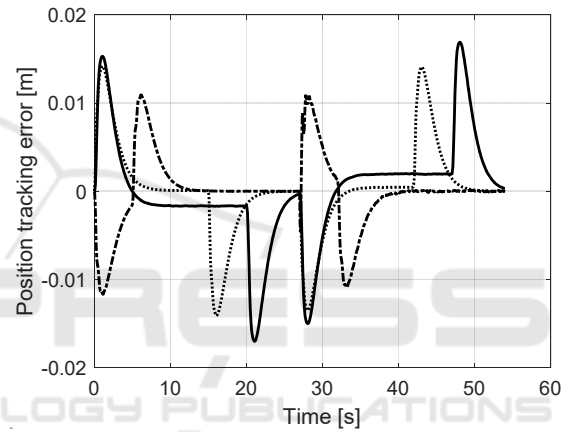


Figure 6: Position tracking error: travel (solid line), traverse (dotted line), and hoist (dash-dot).

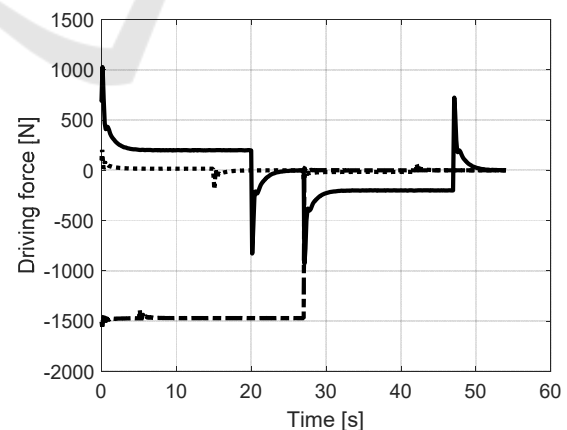


Figure 7: Driving forces: travel (solid line), traverse (dotted line), and hoist (dash-dot).

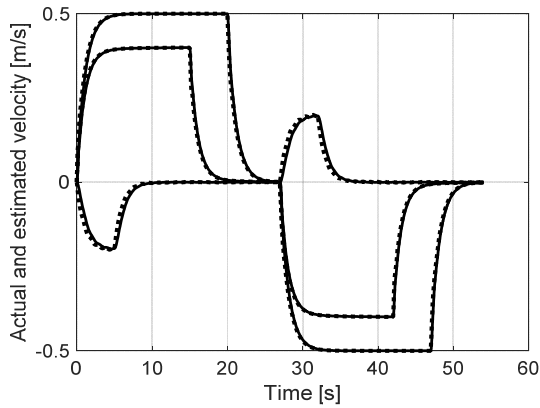


Figure 8: Actual (dotted lines) and observer estimated (solid lines) velocities.

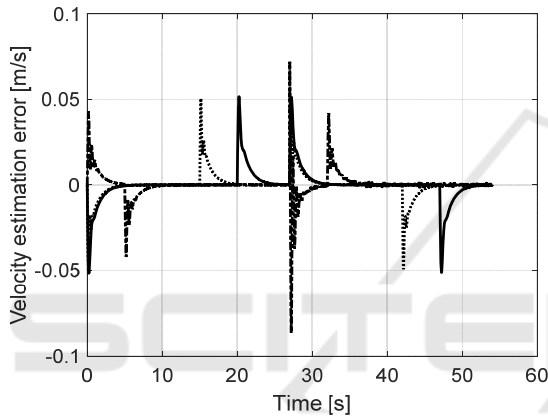


Figure 9: Velocity estimation error: travel ( $\hat{x}$ , solid line), traverse ( $\hat{y}$ , dotted line), and hoist ( $\hat{z}$ , dash-dot).

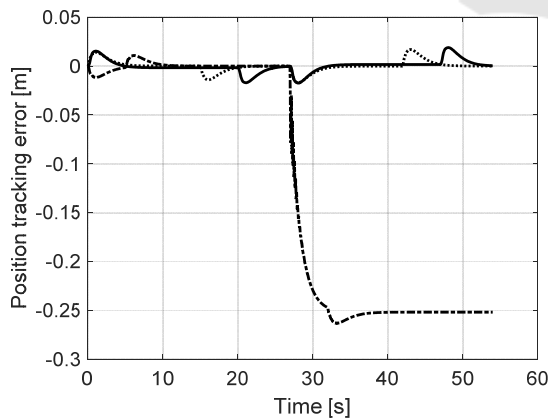


Figure 10: Position tracking error: travel (solid line), traverse (dotted line), and hoist (dash-dot).

## 4 ACTUATOR FAULT SIMULATION AND FAULT ANALYSIS

### 4.1 Actuator Fault Model

Unknown, time-varying actuator fault is described by

$$F^F(t) = \beta(t)F(t) + b(t); t \geq 0 \quad (7)$$

where  $F^F(t)$  is the actuator output force and  $F(t)$  is the control command. The unknown time-varying fault parameters,  $\beta(t)$  and  $b(t)$ , are actuator efficiency factor and the actuator bias fault, respectively. If  $\beta(t) = 1$  and  $b(t) = 0$  for all  $t \geq 0$ , it implies that the actuator always works normally. In practice, actuators have finite actuation effectiveness and bias faults are bounded (Wang et al., 2021). If  $b(t) \neq 0$  and  $0 < \beta(t) < 1$ , it represents an actuator with a bias fault and actuator partial loss-of-control-effectiveness. Actuator fault model in (7) is in compliance with the models used in (Li et al., 2023, Wang et al., 2021, Jin et al., 2022).

In this study, we consider bridge drive motor actuator faults that is directly related to the travel motion in the  $x$ -direction. Actuator loss of control effectiveness,  $1 - \beta$ , that corresponds to the different stages of the unknown actuator fault development from the healthy stage to the final stage are given in Table 1.

Table 1: Stages of actuator fault development.

Stage	Healthy	Early	Progressive 1
$(1 - \beta)\%$	0	5	10
Stage	Progressive 2	Progressive 3	Final
$(1 - \beta)\%$	15	20	25

### 4.2 Health Monitoring and Frequency Domain Analysis

In this paper, we propose overhead crane automatic control and health monitoring with minimally required sensor devices. No sensors are used specifically for health monitoring. Only sensors in the system are the position sensors essential for the feedback control of the 3 degrees-of-freedom of the crane.

We investigate the possibility of using the position tracking error waveform,  $e_x = x - x_d$ , or the difference between the position sensor feedback

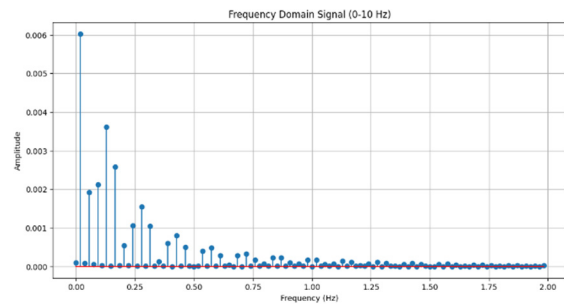
and the desired position to identify and classify the faults. Furthermore, the velocity error waveform or the rate-of-change of error is recommended to better capture the transients related features. However, no velocity sensors are used. Hence, we instead analyse the difference between the observer estimated velocity and the desired velocity ( $\dot{\hat{x}} = \dot{\hat{x}} - \dot{x}_d$ ). To that end, by considering both the waveforms, we intend to combine both the steady-state and transient analysis in the fault diagnosis process.

### 4.3 Features, Correlation, and Sensitivity

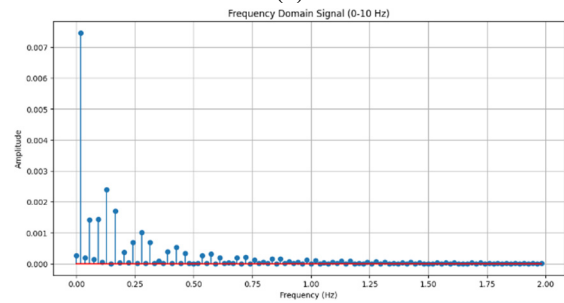
If the crane performs repetitive motions between the same loading and unloading stations, its position and velocity profiles may be considered stationary waveforms. As a result, the position and velocity error waveform are also stationary. Fast Fourier transform (FFT) is a powerful technique to analyse the stationary waveforms. Frequency spectra of the position error waveforms for the healthy actuator and progressive3 stages are given in Fig. 11 and of the velocity error for the same stages are given in Fig. 12. Spectra for the early and final stages are not shown for brevity.

Difference in magnitude of the FFT components between the faulty stage and healthy stage may be used to good effect as the features or inputs to a health monitoring model. Because the values are small, before taking the difference, all FFT component magnitudes are multiplied by a scaling factor of  $10^3$  for better readability and round-off error. In the sequel,  $dh_{p_i}$  denotes the difference in magnitude of the  $i^{th}$  FFT component between the faulty stage and healthy stage of  $e_x = x - x_d$  and  $dh_{v_i}$  denotes that of  $\dot{\hat{x}} = \dot{\hat{x}} - \dot{x}_d$ . For instance,  $i = 0, 1, 2, 3$  represent the DC component, fundamental, 2<sup>nd</sup> harmonic, and 3<sup>rd</sup> harmonic, respectively.

For the purpose of health monitoring, actuator % loss of control effectiveness is taken as the output. When the actuator fault develops slowly over the time,  $e_x$  and  $\dot{\hat{x}}$  waveforms vary in their features yet preserving the stationarity. In this study, we consider the first 100 FFT components of each waveform at all different stages of the actuator fault outlined in Table 1. We first perform Spearman and Kendall Tau correlation analyses to identify the  $dh_{p_i}$  and  $dh_{v_i}$  variables with the strongest correlation with the output. The identified  $dh_{p_i}$  and  $dh_{v_i}$  variables are then ranked according to the range.

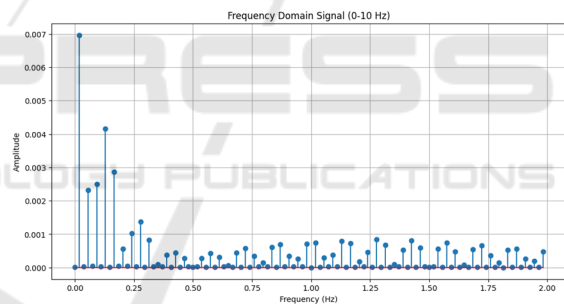


(a)

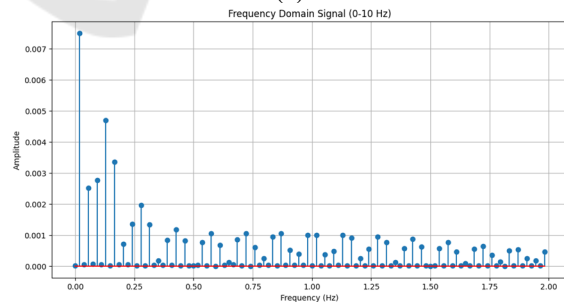


(b)

Figure 11: Position error frequency spectra: (a) Healthy stage (b) Progressive3 stage.



(a)



(b)

Figure 12: Velocity error frequency spectra: (a) Healthy stage (b) Progressive3 stage.

Fig. 12 shows the variation of the  $dh_{p_i}$  and  $dh_{v_i}$  variables that have the highest range. They all have correlation index of either 1 or -1. Here, 1 indicates a perfect positive relationship, -1 indicates a perfect

negative relationship, and 0 indicates no relationship. As it can be seen in Fig. 13, the  $dh_{p_i}$  and  $dh_{v_i}$  variables with the higher range have higher sensitivity. Furthermore, their monotonic and non-linear nature justifies our choice of the type of the correlation, namely, Spearman and Kendall Tau.

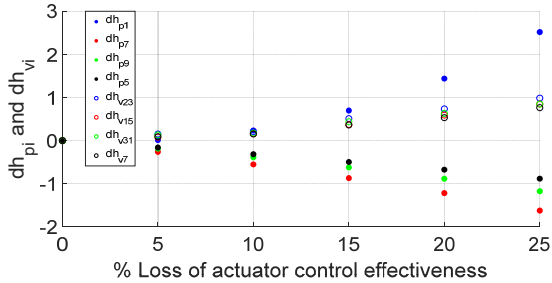


Figure 13: Variation of  $dh_{p_i}$  and  $dh_{v_i}$  with the development of the fault.

Table 2 shows the  $dh_{p_i}$  and  $dh_{v_i}$  variables in the ascending order in terms of the range and sensitivity with the output.

Table 2: The  $dh_{p_i}$  and  $dh_{v_i}$  variables in the ascending order in terms of the range and sensitivity with the output.

Variable	Range	Order of sensitivity	Correlation
$dh_{p1}$	2.51855504	1	+1
$dh_{p7}$	-1.62332400	2	-1
$dh_{p9}$	-1.17462186	3	-1
$dh_{v23}$	0.98634920	4	+1
$dh_{p5}$	-0.88233157	5	-1
$dh_{v15}$	0.84783237	6	+1
$dh_{v31}$	0.84783237	7	+1
$dh_{v7}$	0.84769452	8	+1
$dh_{v17}$	0.76450033	9	+1
$dh_{v25}$	0.73262167	10	+1

Sensitivity analysis helps determine how sensitive the output is to the variations of different inputs. This helps identify which input variable the most critical in the input-output relationship. As seen in Table 2, the highest ranked input variables in terms of sensitivity is a mixture of  $dh_{p_i}$  and  $dh_{v_i}$  variables. Furthermore, in Fig. 13, it can be seen that the sensitivity of  $dh_{p_1}$ , which has the largest range, is small in the early stages of the actuator fault. To this end, we conclude that consideration of the error waveform,  $\hat{x} = \hat{x} - x_d$ , enhances the chances of early detection of the actuator fault.

## 5 CONCLUSIONS

This paper presented a controller-observer scheme for linear position tracking control of the hook-block of an overhead crane in the 3-D space. Closed-loop stability of the plant-controller-linear velocity observer system has been guaranteed using Lyapunov method.

The simple trajectory planning method proposed here has enabled defining the times and distance to the destination, maximum linear velocities and accelerations in the parameters of the function itself as well as ensuring smooth tracking trajectories. This simplifies the meeting of operational and safety requirements and meeting the actuator constraints. Computer numerical simulations in the presence of 15% model parameter uncertainties and random external disturbances have produced small position tracking and velocity estimation errors as well as admissible transient performance.

Using frequency domain, correlation, and sensitivity analysis, we have also shown that position tracking error,  $e_x = x - x_d$ , and velocity error,  $\hat{x} = \hat{x} - \dot{x}_d$ , waveforms may be used successfully for actuator health monitoring. As a result, only the position measurements are required for the entire purpose of automatic control and health monitoring in PdM applications of multi-motor systems.

Future work involves investigation of wavelet transforms, wavelet NNs architectures, and ensemble techniques to address the health monitoring problem when the motion trajectories are non-repetitive.

## ACKNOWLEDGEMENTS

We would like to acknowledge the support extended by the industry sponsor, Electro Metal Pressings Pvt. Ltd and the University of Moratuwa for the assistance in publishing this paper.

## REFERENCES

- Gao, Z., Cecati, C., Ding, SX. (2015). A Survey on Fault Diagnosis and Fault Tolerant Techniques-Part II: Fault Diagnosis with Knowledge-Based and Hybrid/Active Approaches. *IEEE Trans. Industrial Electronics*, Vol. 62, pp. 3768-3774.
- Gowriathan, B., Kiruthihan, N., Ratnayake, KDIN., Logeeshan, V., Kumarawadu, S. (2023). Deep-Learning-Based Non-Intrusive Load Monitoring for 3-Phase Systems. *IEEE Access*, Vol. 11, pp. 49337-49347.

- Ji, L., Xu, Y., Zou, J., Wang, M. (2019). Sensorless Control for PMSM With Novel Back EMF Observer Based on Quasi-PR Controller. In *Int. Conf. Electrical Machines and Systems*, Harbin, China.
- Jin, XZ., Che, WW., Wu, ZG., Zhao, Z. (2022). Adaptive Consensus and Circuitual Implementation of a Class of Faulty Multiagent Systems. *IEEE Trans. Syst., Man, Cybern. Syst.*, vol. 52, no. 1, pp. 226–237.
- Kumarawadu, S., Lee, TT. (2009). Neuroadaptive Output Tracking of Fully Autonomous Road Vehicles With an Observer. *IEEE Trans. Intelligent Transportation Systems*, Vol. 10, pp. 335-345.
- Kumarawadu, S., Watanabe, K., Lee, TT. (2007). High-Performance Object Tracking and Fixation With an Online Neural Observer. *IEEE Trans. Systems, Man, and Cybernetics, Part B (Cybernetics)*, Vol. 37, pp. 213-223.
- Khatamianfar, A. (2015). Advanced Discrete-Time Control Methods for Industrial Applications. PhD Thesis, Cornell Univ. (also available at www.researchgate.net).
- Lee, HH. (1998). Modeling and Control of a Three-Dimensional Overhead Crane. *Journal of Dynamic Systems, Measurement and Control*, Vol. 120, pp. 471-476.
- Li, L., Zhang, Q., Liu, J. (2023). Consensus Tracking and Vibration Control for Multiple Overhead Cranes with Flexible Cables Under Time Varying Actuator Faults. *IEEE Trans. Automation Science and Engineering*, pp. 1-11.
- Wang, C., Wen, C., Guo, L. (2021). Adaptive Consensus Control for Nonlinear Multiagent Systems with Unknown Control Directions and Timevarying Actuator Faults. *IEEE Trans. Autom. Control*, vol. 66, no. 9, pp. 4222–4229.
- Wen JT., Bayard, DS. (1988). New Class of Control Laws for Robot Manipulators:Non-Adaptive Case. *Int. Journal of Control*, vol. 47, pp. 1361–1385.
- Suzuki, K., Fujii, T. (2006). Fault Diagnosis of Parameter Change Type Faults and a Fault Tolerant System Design for Servo Systems. In *American Control Conference*, Minneapolis, Minnesota.

## APPENDIX

Consider the Lyapunov function candidate

$$L = \frac{1}{2}\dot{z}^2 + \lambda\dot{z}z + \frac{1}{2}(L_p + \lambda L_d)\dot{z}^2 + \frac{1}{2}e^2 + \lambda\dot{e}e + \frac{1}{2}(k_p + \lambda k_d)e^2 \quad (A1)$$

which is positive definite for  $\lambda$  sufficiently small. With (4), (5), and dynamics equation, (3), we get

$$M(\ddot{z} + L_d\dot{z} + L_p\dot{z}) = -D\dot{z} - d \quad (A2)$$

$$M(\ddot{e} + k_d\dot{e} + k_p e - k_d\dot{z}) = -D\dot{z} - d \quad (A3)$$

Time differentiating (A1) and using the results (A2), (A3) yield

$$\begin{aligned} \dot{L} = & -\left(L_d + \frac{D}{M} - \lambda\right)\dot{z}^2 - \lambda L_p\dot{z}^2 \\ & - (k_d - \lambda)\dot{e}^2 - \lambda k_p e^2 \\ & - \frac{D}{M}(\lambda\dot{z} + \dot{e} + \lambda e)\dot{z} \\ & - \frac{d}{M}(\dot{z} + \lambda\dot{z} + \dot{e} + \lambda e) \\ & + k_d(\dot{e} + \lambda e)\dot{z} \end{aligned} \quad (A4)$$

Following inequalities can be written for the terms of (A4)

$$\begin{aligned} & -\left(L_d + \frac{D}{M} - \lambda\right)\dot{z}^2 - \lambda L_p\dot{z}^2 - \\ & (k_d - \lambda)\dot{e}^2 - \lambda k_p e^2 \leq 0 \end{aligned} \quad (A5)$$

$$\begin{aligned} & -\frac{D}{M}(\lambda\dot{z} + \dot{e} + \lambda e)\dot{z} \\ & \leq \frac{D}{M}(\lambda|\dot{z}| + |\dot{e}| + \lambda|e|)|\dot{z}| \\ & \leq \frac{D}{2M}(\dot{e}^2 + \lambda e^2 + 3\dot{z}^2 + \lambda^2\dot{z}^2) \end{aligned} \quad (A6)$$

$$\begin{aligned} & -\frac{d}{M}(\dot{z} + \lambda\dot{z} + \dot{e} + \lambda e) \\ & \leq \frac{d_M}{M}(|\dot{z}| + \lambda|\dot{z}| + |\dot{e}| + \lambda|e|) \\ & \leq \frac{d_M}{2M}(\dot{z}^2 + \lambda^2\dot{z}^2 + \dot{e}^2 + \lambda^2 e^2 + 4) \end{aligned} \quad (A7)$$

In (A6) and (A7), the fact that for any real scalars  $a$  and  $b$ ,  $ab \leq (a^2 + b^2)/2$  is used.

$$\begin{aligned} k_d(\dot{e} + \lambda e)\dot{z} & \leq k_d(|\dot{e}| + \lambda|e|)|\dot{z}| \\ & \leq \frac{k_d}{2}(2\dot{z}^2 + \dot{e}^2 + \lambda^2 e^2) \end{aligned} \quad (A8)$$

Because of the inequalities (A5) through (A8), there results

$$\begin{aligned} \dot{L} \leq & -\left(\frac{k_d}{2} - \lambda - \frac{1}{2}\frac{D}{M} - \frac{1}{2}\frac{d_M}{M}\right)\dot{e}^2 \\ & -\left(\lambda k_p - \frac{\lambda^2}{2}k_d - \frac{\lambda^2}{2}\frac{D}{M} - \frac{\lambda^2}{2}\frac{d_M}{M}\right)e^2 \\ & -\left(L_d - k_d - \lambda - \frac{1}{2}\frac{D}{M} - \frac{1}{2}\frac{d_M}{M}\right)\dot{z}^2 \\ & -\left(\lambda L_p + \frac{\lambda^2}{2}\frac{D}{M} - \frac{\lambda^2}{2}\frac{d_M}{M}\right)\dot{z}^2 + 2\frac{d_M}{M} \end{aligned}$$

According to  $\beta$ -ball lemma (Wen and Bayard, 1988), it follows that

$$\dot{L} \leq -\kappa_1\dot{e}^2 - \kappa_2 e^2 - \kappa_3\dot{z}^2 - \kappa_4\dot{z}^2 + 2\frac{d_M}{M}$$

where  $\kappa_i > 0$ ;  $i = 1, 2, 3, 4$  for a  $\lambda$  sufficiently small and suitably chosen set of controller-observer gains,  $k_d, k_p, L_d, L_p > 0$ . This allows us to write



$$-\dot{L}(\dot{e}, e, \dot{z}, \bar{z}) \leq -\kappa L(\dot{e}, e, \dot{z}, \bar{z}) + \gamma$$

for some  $\kappa > 0$ . Here,  $\gamma = 2 \frac{d_M}{M}$ .

Therefore, the Lyapunov function,  $L(\dot{e}, e, \dot{z}, \bar{z})$ , is positive definite outside a compact set of  $\mathcal{O}(\gamma)$  and the closed-loop plant-controller-observer system, (3), (4), (5), is uniformly ultimately bounded (UUB).

